Article

Journal of
Nanoscience and Nanotechnology
Vol. 16, 12321–12325, 2016
www.aspbs.com/jnn

Photocatalytic Properties of $SrTiO_3$ Nanocubes Synthesized Through Molten Salt Modified Pechini Route

Yin Liu[1, 4, *], Qian Qian[1, 2], Jianjun Li[1], Xiaoguang Zhu[3], Mingxu Zhang[1], and Tianshu Zhang[1]

[1] School of Materials Science and Engineering, Anhui University of Science and Technology, Huainan 232001, Anhui, China
[2] Bengbu Design and Research Institute for Glass Industry, China Triumph International Engineering Group Co. Ltd., Bengbu 233018, Anhui, China
[3] Institute of Solid State Physics, Chinese Academy of Sciences, Heifei 230031, Anhui, China
[4] Anhui Engineering Research Centers of High Performance Glass Fiber Reinforced Composites, Huainan 232001, Anhui, China

$SrTiO_3$ nanocubes with 10–40 nm particles size range were synthesized using a molten salt modified Pechini route at temperature range between 480∼800 °C for 2 h. The formation of $SrTiO_3$ nanocubes were monitored by using thermogravity and differential scanning calorimetry (TG-DSC). The low formation temperature was attributed to the enhanced liquid phase diffusion and reaction rate of the molten salt modified Pechini route. Photodegradation of methylene blue was employed to evaluate photocatalytic performance of the $SrTiO_3$ nanocubes. The degradation of methylene blue by the $SrTiO_3$ nanocubes with 20 nm size reached 96% after 7 h UV light irradiation. The photocatalytic behaviour of the $SrTiO_3$ nanocubes was attributed by their nanometer size and band gap, similar to TiO_2.

Keywords: $SrTiO_3$ Nanocubes, Molten Salt, Pechini Route, Photocatalytic Performance.

1. INTRODUCTION

Strontium titanate ($SrTiO_3$) is a typical multifunctional material with special physical and chemical properties. Due to its high dielectric constant, high dispersion rate and good thermal stability, it has been widely used in random access memory devices, oxygen sensors and high voltage capacitors. In addition, the band gap of the $SrTiO_3$ is about 3.2 eV,[1, 2] which is similar to that of TiO_2. The $SrTiO_3$ is therefore one of the promising photocatalysts in production of hydrogen from water,[3] degradation of various organic contaminants[4] and electrode materials for photocatalytic battery and solid oxide full cells.[5, 6]

$SrTiO_3$ powder was conventionally prepared by using solid state reaction method[7] which involve both high temperature treatment and long reaction duration. Moreover, the variation in the valence of Ti could be a problem for the $SrTiO_3$ powder synthesized by using the solid state reaction method. To address this problem,[8–13] the $SrTiO_3$ powders with fine particle sizes have been prepared through various soft chemical synthesis processes, such as sol–gel method, chemical precipitation and Pechini route.[5, 14–17] However, these methods have shown several disadvantages, including complicated procedures, high cost for chemicals and low production yield. It is therefore important to develop simple, economical and large-scale production method for synthesis of $SrTiO_3$ powder. In this respect, the molten salt synthesis is a promising method which has merits like; high reaction selectivity, low processing temperature and short fabrication time.[12, 13] In this paper, we report the synthesis of narrow size distribution $SrTiO_3$ nanocubes that were synthesized by the molten salt modified Pechini route. Microstructure and photocatalytic performance of the $SrTiO_3$ nanocubes were also investigated.

2. EXPERIMENTAL DETAILS

2.1. Material Synthesis

Analytical grade strontium nitrate ($Sr(NO_3)_2$), potassium titanium oxide oxalate dehydrate ($K_2TiO(C_2O_4)_2 \cdot 2H_2O$) and nitric acid ($HNO_3$) were used as raw materials. To obtain the $SrTiO_3$ precursor solutions, $Sr(NO_3)_2$ was dissolved in appropriate amount of distilled water as A solution, while $K_2TiO(C_2O_4)_2 \cdot 2H_2O$ was dissolved in

*Author to whom correspondence should be addressed.

appropriate amount of 1.0 $mol \cdot L^{-1}$ diluted nitric acid to form B solution. The transparent A solution was then slowly poured into the B solution using magnetic stirring to produce precursor solutions. The mixed $SrTiO_3$ precursor solutions were dried at 100 °C for 24 h. The dried gels were then ground into powders and calcined at different temperatures for different time durations. Finally, the obtained powders were washed thoroughly with distilled water and then dried at 100 °C for 24 h.

2.2. Characterization

Thermal decomposition behavior of the precursors was studied by using thermogravity and differential scanning calorimetry (TG-DSC, SDT-2960). Crystalline structure and phase composition of the samples were examined by using X-ray diffraction spectrometer (XRD, Shimadzu LabX XRD-6000) with Cu-Kα radiation. Their morphologies were observed by using scanning electron microscopy (SEM, Nova Nano SEM450) and high resolution transmission electron microscope (HRTEM, JEOL JEM-2010). Average particle size of the sample was measured by using laser diffraction particle size analyzer (LP, Shimadzu, SALD-7101).

2.3. Photocatalytic Performance

Photocatalytic properties of the $SrTiO_3$ nanocubes were evaluated through photodegration of methylene blue (MB) under simulated UV-light with a 300 W Hg lamp at room temperature. In each test, 100 mg $SrTiO_3$ was suspended in 50 mL of 20 mg/L aqueous solution of methylene blue. Before irradiation, the suspensions were ultrasonically treated in the dark for 5 min to achieve high homogeneity. At given time intervals, UV-visible spectra from 400 nm to 800 nm for all the samples were recorded, while remaining concentration of MB was analyzed by using UV-visible spectrophotometer (Shimadzu UV-2600).

3. RESULTS AND DISCUSSION

3.1. Phase Evolution

Figure 1 shows XRD patterns of the $SrTiO_3$ powders synthesized by using the molten salt modified Pechini route at different temperatures for 2 h. It was observed that the characteristic peaks for the $SrCO_3$ and TiO_2 were still detected at 440 °C while single phase $SrTiO_3$ was obtained at 480 °C (JCPDS card no. 35-734). No obvious difference was found among the XRD patterns from the samples calcined from 480 to 800 °C, although the peak density was increased gradually. This sharpening in the peaks revealed the grain growth of specimens during the calcining process.

Figure 2 shows the XRD patterns of the $SrTiO_3$ powder calcined at 500 °C at different times. It was observed that the main phases were $SrCO_3$ and TiO_2, as the precursor was calcined at 500 °C for 30 min. It indicates that the

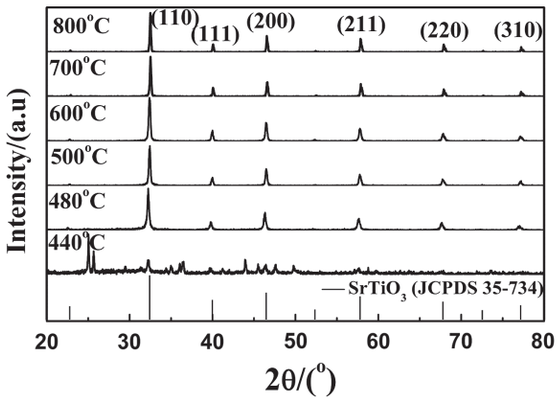

Figure 1. XRD patterns of samples calcined at different temperatures for 2 h.

precursor was firstly decomposed into $SrCO_3$ and TiO_2. By increasing the calcining time to 60 min, the $SrTiO_3$ became the dominant phase together with a small amount of $SrCO_3$ and TiO_2, and when the calcining time was further increased to 120 min, the single phase $SrTiO_3$ was obtained.

3.2. DSC-TG Curves and Reaction Mechanism Analysis

Figure 3 shows DSC/TG curves for the precursor at heating rate of 10 °C/min. It was observed that there were six endothermic peaks and a remarkable exothermic peak. The Endo 1 and Endo 2 peaks observed at 69 °C and 135 °C were associated with evaporation of water. The third endothermic peak (Endo 3) at about 338 °C was attributed to the melting of KNO_3 and the fourth endothermic peak (Endo 4) was maybe due to the decomposition of the precursor. With increasing temperature, the Endo 5 and Endo 6 peaks at about 753 °C and 902 °C were ascribed to the decomposition of potassium carbonate (K_2CO_3) and potassium nitrate (KNO_3), respectively. Correspondingly, there were three stages with obvious weight losses occurred at Endo 1, Endo 4 and Endo 5,

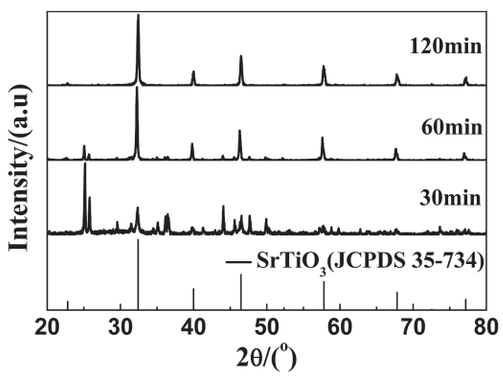

Figure 2. XRD patterns of precursor calcined at 500 °C at different times.

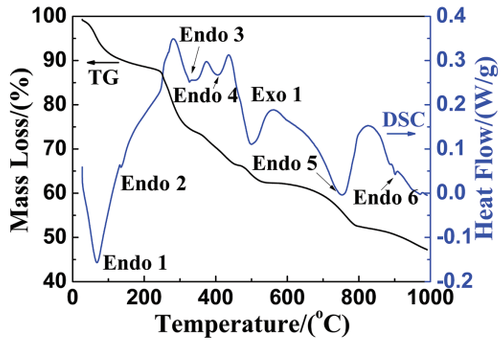

Figure 3. DSC/TG curves for precursor at heating rate 10 °C/min.

respectively. The remarkable exothermic peak with an onset temperature of about 490 °C was centered at 559 °C on the TG/DSC curve. The XRD experiments verified that the perovskite phase $SrTiO_3$ was obtained at 480 °C so the Exo 1 could be ascribed to the formation of $SrTiO_3$.

Based on the XRD and TG-DSC results, the formation mechanism for the $SrTiO_3$ synthesis using the molten salt modified Pechini route can be explained as followed. Firstly, a reaction between $K_2TiO(C_2O_4)_2 \cdot 2H_2O$ and $Sr(NO_3)_2$ in dilute nitric acid solution occurred, as shown in Eq. (1). The main ingredients for the precursor were the polymer molecules

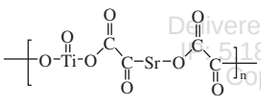

and KNO_3. The KNO_3 reacted as the molten salt at low calcining temperatures, and also as the oxidizing agent for the precursor. The polymer molecules

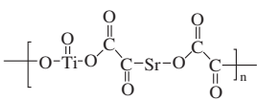

were decomposed into $SrCO_3$, TiO_2 and CO_2 as the temperature reached 400 °C (Eq. (2)). Meanwhile, the $SrTiO_3$ was crystallized from the KNO_3 molten salt solution. K_2CO_3 and KNO_3 were further decomposed into K_2O, NO_2 and CO_2 with increasing calcining temperature, as illustrated in Eq. (3). The formation rate for the $SrTiO_3$ was accelerated due to the presence of K_2O and K_2CO_3 molten salts.

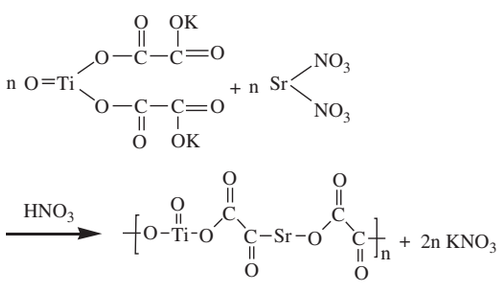

(1)

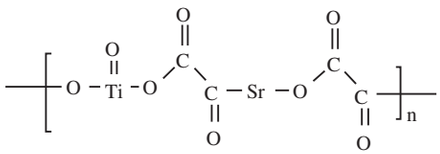

$$\rightarrow TiO_2 + SrCO_3 + CO_2\uparrow \quad (2)$$

$$TiO_2 + SrCO_3 + 2KNO_3 \rightarrow SrTiO_3 + K_2O + 2NO_2\uparrow + CO_2\uparrow \quad (3)$$

3.3. Microstructure

Figure 4 shows SEM images of the samples calcined at different temperatures for 2 h. It can be seen that the average size for the samples was around 10∼40 nm (Seen in Figs. 4(a–c)). A few agglomerated particles are also seen, which may be ascribed to the intense surface effect of the nanosized materials. As the calcining temperature for the samples was up to 800 °C, the $SrTiO_3$ sample consisted mainly of cubic particles with the average size being ∼0.3 μm (Fig. 4(d)).

Figure 5(a) shows TEM image of the $SrTiO_3$ nanocubes calcined at 500 °C. It can be seen that the samples with narrow size distribution were relatively fine, although there was slight particle agglomeration. The average size was about 30 nm, which was consistent with the SEM results. Figure 5(b) depicts HRTEM image of the sample. The plane spacing that corresponded to (100) and (110) of the $SrTiO_3$ could also be clearly observed. The corresponding selected area for electron diffraction (SAED) pattern exhibited diffuse rings (Fig. 5(c)), indicating that the $SrTiO_3$ nanocubes were of polycrystalline nature.

Figure 6 shows particle size distribution curves for the samples obtained at different temperatures for 2 h.

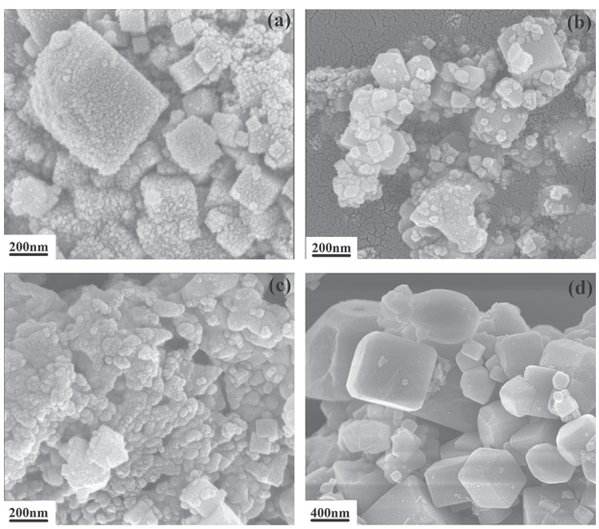

Figure 4. SEM images of $SrTiO_3$ powders calcined at different temperatures for 2 h: (a) 500 °C, (b) 600 °C, (b) 700 °C and (d) 800 °C.

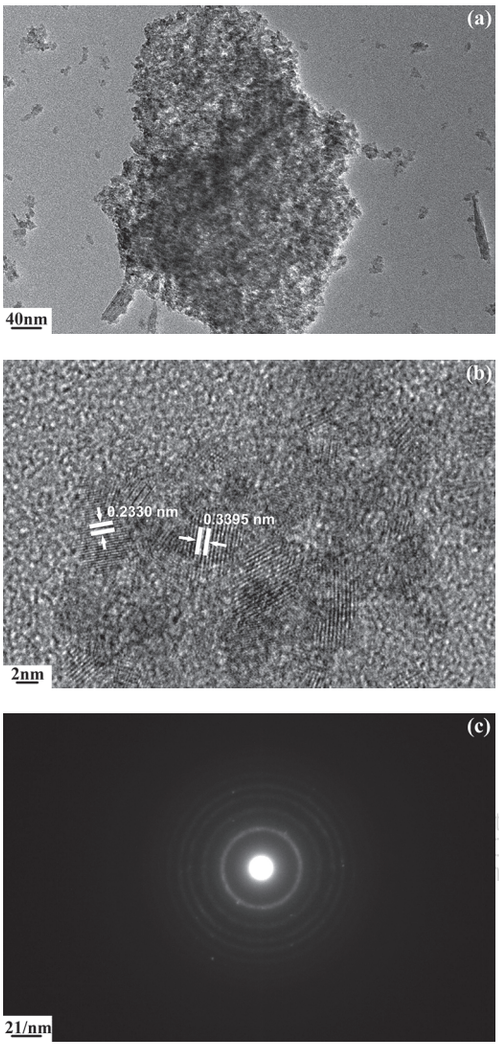

Figure 5. TEM images and SAED pattern for $SrTiO_3$ nanocubes calcined at 500 °C for 2 h: (a) Panoramic view, (b) HRTEM image and (c) SAED pattern.

The three samples had similar particle size distribution in the range of 10–40 nm. In this range (500–700 °C), the effect of temperature on the average particle size (d_{50}) and particle size distribution was not very significant.

Figure 7 shows specific surface area of the $SrTiO_3$ nanocubes calcined at different temperatures. It was found that the specific surface area for the samples decreased from 65.73 to 9.38 m^2/g as the temperature was increased from 500 to 800 °C. Correspondingly, the particle size for the samples increased rapidly from 17.84 to 120.9 nm according to the BET analysis results.

3.4. Photocatalytic Activity

Figure 8(a) shows U-vis absorption spectra of methylene blue solution (initial concentration: 20 mg/L) with 100 mg of $SrTiO_3$ nanocubes calcined at 500 °C for 2 h as photocatalyst exposed to UV light irradiation at

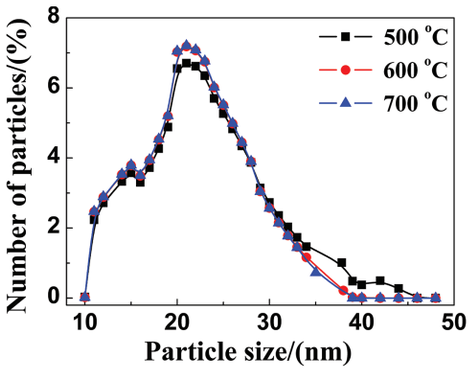

Figure 6. Particle size distribution curves for samples calcined at different temperatures for 2 h.

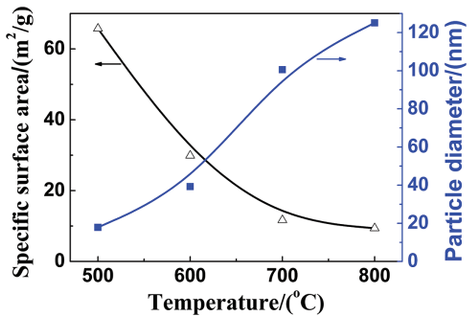

Figure 7. Specific surface area and equivalent particle size for $SrTiO_3$ nanocubes versus calcination temperature.

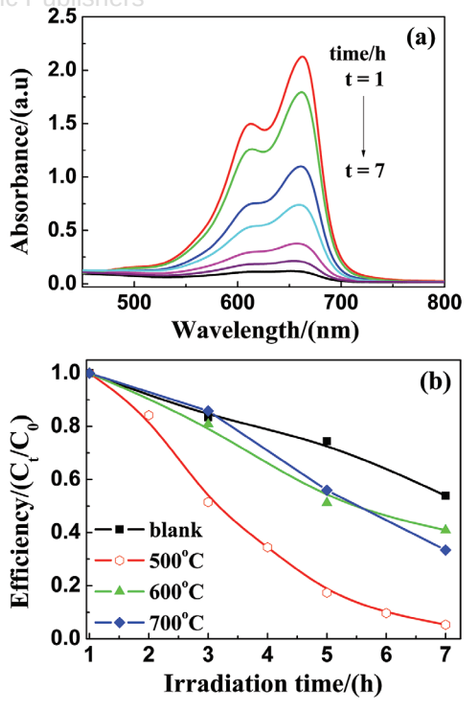

Figure 8. (a) Absorption spectra for MB solution in the presence of $SrTiO_3$ nanocubes calcined at 500 °C for 2 h. (b) Degradation efficiencies for MB solution in the presence of the $SrTiO_3$ nanocubes calcined at different temperatures.

various times. The characteristic absorption of methylene blue at the wavelength of 660 nm decreased rapidly with increasing exposure time and almost completely disappeared after 7 h. Figure 8(b) shows the results for methylene blue degradation by the $SrTiO_3$ nanocubes calcined at the different temperatures, where the ratio of C_t/C_0 (C_t and C_0 are the reaction and initial concentrations of methylene) represented the degree of degradation. A blank test under UV light irradiation exhibited the weak degradation of methylene blue. For the $SrTiO_3$ nanocubes calcined at 500 °C, the degradation of methylene blue reached 96% after 7 h. Also, the degradation of methylene blue decreases with increasing calcinning temperature for the $SrTiO_3$ nanocubes. The photocatalytic behaviour of $SrTiO_3$ nanocubes was possibly attributed to the effect of their nanometer size[18–21] and band gap, similar to that of TiO_2.[22–28]

4. CONCLUSIONS

Perovskite $SrTiO_3$ nanocubes with particle size in the range of 10–40 nm were synthesized through a molten salt modified Pechini route. Single phase $SrTiO_3$ was formed at 480 °C. Methylene blue could be almost completely degraded by using the $SrTiO_3$ nanocubes calcined at 500 °C for 2 h, as the photocatalyst.

Acknowledgment: This work was supported by China Postdoctoral Science Foundation (2014M550337), Natural Science Foundation of High Education School of Anhui Province (KJ2013A091), Science and Technology Project of Anhui Province (1604a0802122) and Fund of Key Laboratory of Optoelectronic Materials Chemistry and Physics, Chinese Academy of Sciences.

References and Notes

1. C. Chang, B. Ray, D. K. Paul, D. Demydov, and K. J. Klabunde, *J. Mol. Catal. A-Chem.* 281, 99 (**2008**).
2. F. Zou, Z. Jiang, X. Q. Qin, Y. X. Zhao, L. Y. Jiang, J. F. Zhi, T. C. Xiao, and P. P. Edwards, *Chem. Commun.* 48, 8514 (**2012**).
3. H. W. Kang, S. N. Lim, D. G. Song, and S. B. Park, *Int. J. Hydrogen Energ.* 37, 11602 (**2012**).
4. A. Z. Jia, X. Q. Liang, Z. Q. Su, T. Zhu, and S. X. Liu, *J. Hazardous Mater.* 178, 233 (**2010**).
5. M. Mori, K. Nakamura, and T. Itoh, *J. Fuel. Cell Sci. Tech.* 9, 21007 (**2012**).
6. X. Li, H. L. Zhao, F. Gao, N. Chen, and N. S. Xu, *Electrochem. Commun.* 10, 1567 (**2008**).
7. X. Li, H. L. Zhao, W. Shen, F. Gao, X. L. Huang, Y. Li, and Z. M. Zhu, *J. Power Sources* 166, 47 (**2007**).
8. T. Puangpetch, T. Sreethawong, S. Yoshikawa, and S. Chavadej, *J. Molec. Cataly. A-Chem.* 287, 70 (**2008**).
9. H. Yu, S. X. Ouyang, and S. C. Yan, *J. Mater. Chem.* 21, 11347 (**2011**).
10. H. L. Li, Z. N. Du, G. L. Wang, and Y. C. Zhang, *Mater. Lett.* 64, 431 (**2010**).
11. Y. F. Liu, Y. N. Lu, M. Xu, L. F. Zhou, and S. Z. Shi, *Mater. Chem. Phys.* 114, 37 (**2009**).
12. Y. H. Chen and Y. D. Chen, *J. Hazardous Mater.* 185, 168 (**2011**).
13. J. S. Wang, S. Yin, and T. Sato, *J. Photoch. Photobio. A* 187, 72 (**2007**).
14. Ľ. Bača, Z. Lenčéš, and N. Stelzer, *J. Eur. Ceram. Soc.* 31, 1465 (**2011**).
15. S. J. Qiu, C. Gao, X. D. Zheng, J. Chen, C. N. Yang, X. X. Gan, and H. Q. Fan, *J. Mater. Sci.* 43, 3094 (**2008**).
16. M. R. S. Silva, L. E. B. Soledade, S. J. G. Lima, E. Longo, A. G. Souza, and Iêda M. G. Santos, *J. Therm. Analy. Calor.* 87, 731 (**2007**).
17. F. Fujishiro, T. Arakawa, and T. Hashimoto, *Mater. Lett.* 65, 1819 (**2011**).
18. S. C. Yan, L. Y. Zhou, Y. Shi, Z. L. Cao, D. Hu, and X. Xu, *J. Green Sci. Technol.* 1, 131 (**2013**).
19. D. Van Thuan, N. T. Khoa, S. W. Kim, D. Yoo, E. J. Kim, and S. H. Hahn, *J. Nanosci. Nanotechnol.* 15, 8896 (**2015**).
20. J. Tang, B. Zhou, S. L. Zhang, Z. Wang, L. Xiong, and P. Li, *Sci. China Chem.* 58, 858 (**2015**).
21. X. L. Li, X. M. Mao, X. C. Zhang, Y. F. Wang, Y. W. Wang, H. Zhang, X. G. Hao, and C. M. Fan, *Sci. China Chem.* 58, 457 (**2015**).
22. Z. Q. Cheng, D. Ding, X. K. Nie, Y. T. Xu, Z. L. Song, T. Fu, Z. Chen, and W. H. Tan, *Sci. China Chem.* 58, 1131 (**2015**).
23. Y. Peng, M. H. Li, S. J. Zhang, G. Z. Nie, M. Qi, and B. C. Pan, *Sci. China Chem.* 58, 1211 (**2015**).
24. M. Shamalah, R. S. L. Aparna, R. G. S. V. Prasad, and A. R. Phani, *J. Green Sci. Technol.* 1, 14 (**2013**).
25. V. Loryuenyong, J. Charoensuk, R. Charupongtawitch, A. Usakulwattana, and A. Buasri, *J. Nanosci. Nanotechnol.* 16, 296 (**2016**).
26. Y. Song, N. Cho, M. Lee, B. Kim, and D. Y. Lee, *J. Nanosci. Nanotechnol.* 16, 1831 (**2016**).
27. D. Nguyen and S. Hong, *J. Nanosci. Nanotechnol.* 16, 1911 (**2016**).
28. W. Wu, *J. Green Sci. Technol.* 1, 107 (**2013**).

Received: 16 July 2015. Accepted: 5 March 2016.